



Thermal Buckling Analysis of Circular Bilayer Graphene Sheets Resting on an Elastic Matrix Based on Nonlocal Continuum Mechanics

M. Ahmad Pour¹, M.E. Golmakani¹ , M. Malikan^{1,2} 

¹ Department of Mechanical Engineering, Islamic Azad University, Mashhad Branch, P.O.B. 9187144123, Mashhad, Iran

² Department of Mechanics of Materials and Structures, Faculty of Civil and Environmental Engineering
Gdansk University of Technology, Gdansk, Poland

Received October 09 2019; Revised November 08 2019; Accepted for publication November 12 2019.

Corresponding author: M.E. Golmakani (m.e.golmakani@mshdiau.ac.ir)

© 2020 Published by Shahid Chamran University of Ahvaz

& International Research Center for Mathematics & Mechanics of Complex Systems (M&MoCS)

Abstract. In this article, the thermal buckling behavior of orthotropic circular bilayer graphene sheets embedded in the Winkler–Pasternak elastic medium is scrutinized. Using the nonlocal elasticity theory, the bilayer graphene sheets are modeled as a nonlocal double-layered plate that contains small scale effects and van der Waals (vdW) interaction forces. The vdW interaction forces between the layers are simulated as a set of linear springs using the Lennard–Jones potential model. Using the principle of virtual work, the set of equilibrium equations are obtained based on the first-order shear deformation theory (FSDT) and nonlocal differential constitutive relation of Eringen. Differential quadrature method (DQM) is employed to solve the governing equations for simply-supported and clamped boundary conditions. Finally, the effects of the small scale parameter, vdW forces, aspect ratio, elastic foundation, and boundary conditions are considered in detail.

Keywords: Thermal buckling; Bilayer graphene sheets; Elastic medium; Nonlocal elasticity; van der Waals forces; First-order shear deformation theory; Differential quadrature method

1. Introduction

Throughout the past few years, graphene sheets have enticed researchers tremendously due to their extraordinary electronic, thermal and mechanical properties which make it a reliable candidate for pervasive applications in many fields such as superfast microelectronics, micro-electro-mechanical systems (MEMS), nano-electromechanical systems (NEMS), biomedical, bioelectrical, reinforcement role at composites and etc. [1-6]. Owing to their broad range of applications, predicting the mechanical behavior of graphene sheets is of great importance. However, compared to the mechanical analysis of one-dimensional nanostructures such as nanobeams, nanorods and carbon nanotubes (CNTs), we cannot neglect the van der Waals interaction between the atoms and its inner distance in contrast with the main physics of problem [7]. In recent years, various size-dependent continuum theories such as couple stress theory [8], strain gradient elasticity theory [9-12], modified couple stress theory [13-23], nonlocal elasticity theory [24-41] and nonlocal strain gradient theories (higher and lower-order) [42-48] are proposed. These theories are comprised of information about the interatomic forces and internal lengths that are introduced as small scale effects in nonlocal elasticity theory [27]. Amidst them, it is proved that the nonlocal elasticity theory of Eringen [24-27] in micro and nano-materials has outshined among the nanotechnology community owing to its simplicity, high reliability and close agreement with molecular dynamics (MD) simulations for mechanical analysis of nanostructures. In recent years, a lot of studies have

been carried out to predict the vibrations, buckling and bending analyses [49-70] of nanostructures with several geometries based on nonlocal elasticity theory. In order to improve the stiffness and strength of a graphene sheet, multilayers of graphene sheets (MLGSs) have been produced. In order to make MLGSs, several SLGs are set on each other by weak van der Waals (vdW) bonds between the surface atoms [71]. Moreover, the bilayer graphene sheets (BLGS) can be modeled as a nonlocal double-layered plate which contains vdW interaction forces and the small scale effect. Owing to the superior advantages of MLGS, some works have also been conducted to study their mechanical behaviors i.e. bending [71-72], vibration [73-76], and buckling [77-80]. According to the literature, some research works have been presented to analyze the mechanical behaviors of rectangular MLGSs using nonlocal elasticity theory. However, in comparison with rectangular graphene sheets, research studies of nanoplates with circular geometry are limited in number [81].

This study considers the thermal buckling of circular bilayer graphene sheets on a two-parameter elastic foundation using the first-order shear deformation theory (FSDT) and nonlocal differential constitutive relation of Eringen. The governing equations are obtained in terms of displacement variables and then solved using the differential quadrature method (DQM) for different boundary conditions. The obtained results of the DQM are highly consistent with those of other works for simplified cases. Finally, influences of small scale parameter, thickness and radius of circular BLGS, elastic foundation and boundary conditions are studied on the thermal buckling load in detail.

2. Governing Equations

The geometry and coordinate system of circular BLGS with thickness h and radius r are shown in Fig. 1.

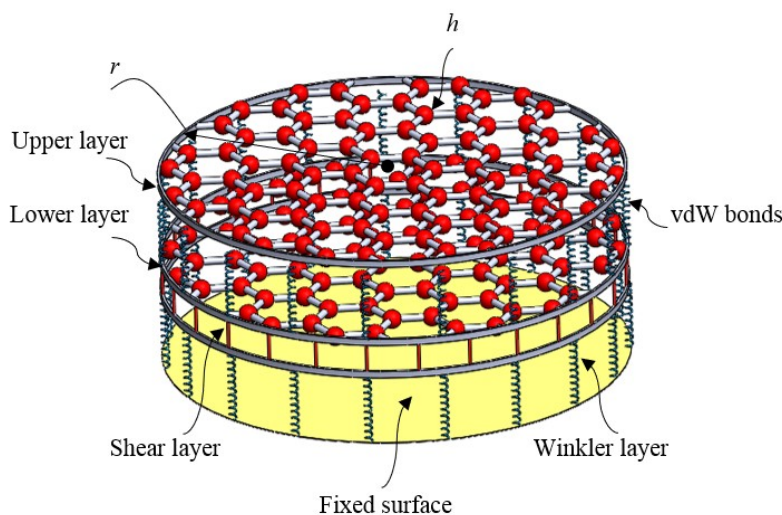


Fig. 1. The circular bilayer graphene sheets in an atomic schema bridged on an elastic foundation

According to the FSDT, the displacement field can be defined as follows:

$$\begin{aligned}
 U(r, \theta, z) &= u(r) + z\phi(r) \\
 V(r, \theta, z) &= 0 \\
 W(r, \theta, z) &= w(r)
 \end{aligned}
 \tag{1}$$

where u and w are the displacement components of the mid-plane along the radial and vertical displacements, respectively. Also, ϕ denotes the rotational function of the transverse normal about the r -axis. The von Kármán strain fields are used as follows:

$$\begin{aligned}
 \epsilon_r &= \frac{\partial U}{\partial r} + \frac{1}{2} \left(\frac{\partial W}{\partial r} \right)^2 \\
 \epsilon_\theta &= \frac{U}{r} \\
 \gamma_{rz} &= \frac{\partial U}{\partial z} + \frac{\partial W}{\partial r}
 \end{aligned}
 \tag{2}$$

where ϵ_r and ϵ_θ are the normal strains and γ_{rz} is the shear strain. In nonlocal elasticity theory, the effects of small scale and interatomic bonds are included in the constitutive equations as material parameters [24]. Eringen presented a differential form of the nonlocal constitutive equation from nonlocal balance law as follows [26-27]:

$$(1 - \mu \nabla^2) \sigma^{NL} = \sigma^L = C \epsilon, \quad \mu (nm)^2 = (e_0 a)^2
 \tag{3}$$

$$C = \begin{bmatrix} \frac{E_1}{1-\nu_{12}\nu_{21}} & \frac{\nu_{12}E_2}{1-\nu_{12}\nu_{21}} & 0 \\ \frac{\nu_{12}E_2}{1-\nu_{12}\nu_{21}} & \frac{E_2}{1-\nu_{12}\nu_{21}} & 0 \\ 0 & 0 & G_{23} \end{bmatrix} \quad (4)$$

in which E_1 and E_2 are elasticity moduli along r and θ directions, G_{23} is shear modulus, ν_{12} and ν_{21} are Poisson's ratio for the orthotropic plate. Furthermore, index L defines local and index NL shows nonlocal components. Additionally, the parameters σ and ε represent the static stresses and strains. Also, a is an internal characteristic length and e_0 is a material constant that should be defined by experiment. The parameter $e_0 a$ is the small scale parameter revealing the small scale effect on the responses of nanosize structures. The value of the small scale parameter depends on boundary condition, chirality, mode shapes, number of walls, and the nature of motions. The nonlocal stresses can be defined by using eq. (3), in addition, ∇^2 expresses the Laplacian operator which is defined for axisymmetric conditions as follows:

$$\nabla^2 = \frac{d^2}{dr^2} + \frac{1}{r} \frac{d}{dr} \quad (5)$$

The nonlocal force, moment and shear force components, namely N_r^{NL} , N_θ^{NL} , M_r^{NL} , M_θ^{NL} and Q_r^{NL} , are introduced as follows:

$$\begin{aligned} \begin{Bmatrix} N_r \\ N_\theta \end{Bmatrix}^{NL} &= \int_{-\frac{h}{2}}^{\frac{h}{2}} \begin{Bmatrix} \sigma_r \\ \sigma_\theta \end{Bmatrix}^{NL} dz \\ \begin{Bmatrix} M_r \\ M_\theta \end{Bmatrix}^{NL} &= \int_{-\frac{h}{2}}^{\frac{h}{2}} \begin{Bmatrix} \sigma_r \\ \sigma_\theta \end{Bmatrix}^{NL} z dz \\ Q_r^{NL} &= k \times \int_{-\frac{h}{2}}^{\frac{h}{2}} \sigma_{rz}^{NL} dz \end{aligned} \quad (6)$$

By substituting stress values into resultant forces, the following constitutive relations are obtained:

$$\begin{aligned} N_r^L &= \left(Q_{11}^0 \varepsilon_r + Q_{12}^0 \varepsilon_\theta \right) h - N_r^T \\ N_\theta^L &= \left(Q_{12}^0 \varepsilon_r + Q_{22}^0 \varepsilon_\theta \right) h - N_\theta^T \\ M_r^L &= \left(Q_{11}^1 \varepsilon_r + Q_{12}^1 \varepsilon_\theta \right) \frac{h^3}{12} - M_r^T \\ M_\theta^L &= \left(Q_{12}^1 \varepsilon_r + Q_{22}^1 \varepsilon_\theta \right) \frac{h^3}{12} - M_\theta^T \\ Q_r^L &= C_{44}^0 \gamma_{rz} h \end{aligned} \quad (7)$$

in which N_r^T , N_θ^T , M_r^T , and M_θ^T are the thermal and moment stress resultants along the radius and angle of the circular plate. Moreover, the stiffness parameters of the material are as follows:

$$Q_{11} = \frac{E_1}{1-\nu_{12}\nu_{21}}, \quad Q_{22} = \frac{E_2}{1-\nu_{12}\nu_{21}}, \quad Q_{12} = \frac{\nu_{12}E_2}{1-\nu_{12}\nu_{21}}, \quad C_{44} = kG_{23} \quad (8)$$

where k defines a factor in order to refine the distribution of the shear stress along the thickness of the sheet. By computing strains and substituting the values of the stiffness matrix (Eq. (8)) in terms of material constants, the following relations are obtained:

$$\begin{aligned} N_r^L &= \frac{E_1 h}{1-\nu_{12}\nu_{21}} \left(\frac{\partial u}{\partial r} + \frac{1}{2} \left(\frac{\partial w}{\partial r} \right)^2 \right) + \frac{\nu_{12} E_2 h}{1-\nu_{12}\nu_{21}} \frac{u}{r} - N_r^T \\ N_\theta^L &= \frac{\nu_{12} E_2 h}{1-\nu_{12}\nu_{21}} \left(\frac{\partial u}{\partial r} + \frac{1}{2} \left(\frac{\partial w}{\partial r} \right)^2 \right) + \frac{E_2 h}{1-\nu_{12}\nu_{21}} \frac{u}{r} - N_\theta^T \end{aligned} \quad (9)$$

$$\begin{aligned}
 M_r^L &= \frac{E_1 h^3}{12(1-\nu_{12}\nu_{21})} \frac{\partial \phi}{\partial r} + \frac{\nu_{12} E_2 h^3}{12(1-\nu_{12}\nu_{21})} \frac{1}{r} \phi - M_r^T \\
 M_\theta^L &= \frac{\nu_{12} E_2 h^3}{12(1-\nu_{12}\nu_{21})} \frac{\partial \phi}{\partial r} + \frac{E_2 h^3}{12(1-\nu_{12}\nu_{21})} \frac{1}{r} \phi - M_\theta^T \\
 Q_r^L &= kG_{23} h \left(\frac{\partial w}{\partial r} + \phi \right)
 \end{aligned} \tag{9}$$

Using the principle of minimum total potential energy, for a system to be in an equilibrium state, the variation of total potential energy needs to be equal to zero as:

$$\delta \Pi = \delta S + \delta \Omega = 0 \tag{10}$$

in which S and Ω denote the strain energy and the work done by the externally applied forces, respectively, which are defined as follows:

$$\delta S = \iiint_V (\sigma_r \delta \varepsilon_r + \sigma_\theta \delta \varepsilon_\theta + \sigma_{rz} \delta \gamma_{rz}) dV \tag{11}$$

In continuation, the work done by the external forces can be written in the following relations (Note that index 1 defines upper layer and index 2 is allocated for the lower layer):

$$\delta \Omega_1 = \iint_A \left(k_0 (w_1 - w_2) (\delta w_1) + N \frac{\partial}{\partial r} (\delta u_1) \right) r dr d\theta \tag{12a}$$

$$\delta \Omega_2 = \iint_A \left((k_0 (w_2 - w_1) - k_w w_2 + k_p \nabla^2 w_2) (\delta w_2) + N \frac{\partial}{\partial r} (\delta u_2) \right) r dr d\theta \tag{12b}$$

where δ is the variation symbol, also, k_w , k_p and k_0 are the Winkler and Pasternak stiffness coefficients of the elastic foundation and van der Waals interaction forces, respectively. By using the nonlocal stress resultants in Eqs. (6) and energy relations in Eqs. (10-12), the nonlocal governing equations can be defined as follows in eqs. (13) and (14). It is noted that Eqs. (13) are corresponding to the upper layer and Eqs. (14) are related to the lower layer:

$$\begin{aligned}
 \frac{1}{r} N_{r1}^{NL} + \frac{\partial N_{r1}^{NL}}{\partial r} - \frac{1}{r} N_{\theta1}^{NL} &= 0 \\
 k_0 (w_1 - w_2) + N_\theta^{th} \frac{1}{r} \frac{\partial w_1}{\partial r} + N_r^{th} \frac{\partial^2 w_1}{\partial r^2} + \frac{\partial Q_{r1}^{NL}}{\partial r} + \frac{1}{r} Q_{r1}^{NL} &= 0 \\
 \frac{\partial M_{r1}^{NL}}{\partial r} + \frac{1}{r} M_{r1}^{NL} - \frac{1}{r} M_{\theta1}^{NL} - Q_{r1}^{NL} &= 0
 \end{aligned} \tag{13}$$

$$\begin{aligned}
 \frac{1}{r} N_{r2}^{NL} + \frac{\partial N_{r2}^{NL}}{\partial r} - \frac{1}{r} N_{\theta2}^{NL} &= 0 \\
 k_0 (w_2 - w_1) - k_w w_2 + k_p \nabla^2 w_2 + N_\theta^{th} \frac{1}{r} \frac{\partial w_2}{\partial r} + N_r^{th} \frac{\partial^2 w_2}{\partial r^2} + \frac{\partial Q_{r2}^{NL}}{\partial r} + \frac{1}{r} Q_{r2}^{NL} &= 0 \\
 \frac{\partial M_{r2}^{NL}}{\partial r} + \frac{1}{r} M_{r2}^{NL} - \frac{1}{r} M_{\theta2}^{NL} - Q_{r2}^{NL} &= 0
 \end{aligned} \tag{14}$$

Using Eqs. (9, 13 and 14) leads to the following relations:

$$\begin{aligned}
 \frac{1}{r} \left(\frac{E_1 h}{1-\nu_{12}\nu_{21}} \left(\frac{\partial u_1}{\partial r} + \frac{1}{2} \left(\frac{\partial w_1}{\partial r} \right)^2 \right) + \frac{\nu_{12} E_2 h}{1-\nu_{12}\nu_{21}} \frac{u_1}{r} - N_r^T \right) + \frac{E_1 h}{1-\nu_{12}\nu_{21}} \left(\frac{\partial^2 u_1}{\partial r^2} + \frac{\partial w_1}{\partial r} \frac{\partial^2 w_1}{\partial r^2} \right) + \frac{\nu_{12} E_2 h}{1-\nu_{12}\nu_{21}} \left(\frac{1}{r} \frac{\partial u_1}{\partial r} - \frac{u_1}{r^2} \right) \\
 - \frac{1}{r} \left(\frac{\nu_{12} E_2 h}{1-\nu_{12}\nu_{21}} \left(\frac{\partial u_1}{\partial r} + \frac{1}{2} \left(\frac{\partial w_1}{\partial r} \right)^2 \right) - \frac{E_2 h}{1-\nu_{12}\nu_{21}} \frac{u_1}{r} + N_\theta^T \right) = 0
 \end{aligned} \tag{15}$$

$$(1 - \mu \nabla^2) \left(k_0 (w_1 - w_2) + N_\theta^{th} \frac{1}{r} \frac{\partial w_1}{\partial r} + N_r^{th} \frac{\partial^2 w_1}{\partial r^2} \right) + kG_{23} h \left(\frac{\partial^2 w_1}{\partial r^2} + \frac{\partial \phi}{\partial r} \right) + \frac{1}{r} kG_{23} h \left(\frac{\partial w_1}{\partial r} + \phi \right) = 0 \tag{16}$$

$$\frac{E_1 h^3}{12(1-\nu_{12}\nu_{21})} \frac{\partial^2 \phi_1}{\partial r^2} + \frac{\nu_{12} E_2 h^3}{12(1-\nu_{12}\nu_{21})} \frac{1}{r} \left(\frac{\partial \phi_1}{\partial r} - \frac{\phi_1}{r} \right) + \frac{1}{r} \left(\frac{E_1 h^3}{12(1-\nu_{12}\nu_{21})} \frac{\partial \phi_1}{\partial r} + \frac{\nu_{12} E_2 h^3}{12(1-\nu_{12}\nu_{21})} \frac{\phi_1}{r} \right) - \frac{1}{r} \left(\frac{\nu_{12} E_2 h^3}{12(1-\nu_{12}\nu_{21})} \frac{\partial \phi_1}{\partial r} - \frac{E_2 h^3}{12(1-\nu_{12}\nu_{21})} \frac{\phi_1}{r} \right) - k G_{23} h \left(\frac{\partial w_1}{\partial r} + \phi_1 \right) = 0 \quad (17)$$

$$\frac{1}{r} \left(\frac{E_1 h}{1-\nu_{12}\nu_{21}} \left(\frac{\partial u_2}{\partial r} + \frac{1}{2} \left(\frac{\partial w_2}{\partial r} \right)^2 \right) + \frac{\nu_{12} E_2 h}{1-\nu_{12}\nu_{21}} \frac{u_2}{r} - N_r^T \right) + \frac{E_1 h}{1-\nu_{12}\nu_{21}} \left(\frac{\partial^2 u_2}{\partial r^2} + \frac{\partial w_2}{\partial r} \frac{\partial^2 w_2}{\partial r^2} \right) + \frac{\nu_{12} E_2 h}{1-\nu_{12}\nu_{21}} \frac{1}{r} \left(\frac{\partial u_2}{\partial r} - \frac{u_2}{r} \right) - \frac{1}{r} \left(\frac{\nu_{12} E_2 h}{1-\nu_{12}\nu_{21}} \left(\frac{\partial u_2}{\partial r} + \frac{1}{2} \left(\frac{\partial w_2}{\partial r} \right)^2 \right) - \frac{E_2 h}{1-\nu_{12}\nu_{21}} \frac{u_2}{r} + N_\theta^T \right) = 0 \quad (18)$$

$$(1-\mu \nabla^2) \left(k_0 (w_2 - w_1) - k_w w_2 + k_p \nabla^2 w_2 \right) + k G_{23} h \left(\frac{\partial^2 w_2}{\partial r^2} + \frac{\partial \phi_2}{\partial r} \right) + k G_{23} h \frac{1}{r} \left(\frac{\partial w_2}{\partial r} + \phi_2 \right) = 0 \quad (19)$$

$$\frac{E_1 h^3}{12(1-\nu_{12}\nu_{21})} \frac{\partial^2 \phi_2}{\partial r^2} + \frac{\nu_{12} E_2 h^3}{12(1-\nu_{12}\nu_{21})} \frac{1}{r} \left(\frac{\partial \phi_2}{\partial r} - \frac{\phi_2}{r} \right) + \frac{1}{r} \left(\frac{E_1 h^3}{12(1-\nu_{12}\nu_{21})} \frac{\partial \phi_2}{\partial r} + \frac{\nu_{12} E_2 h^3}{12(1-\nu_{12}\nu_{21})} \frac{\phi_2}{r} \right) - \frac{1}{r} \left(\frac{\nu_{12} E_2 h^3}{12(1-\nu_{12}\nu_{21})} \frac{\partial \phi_2}{\partial r} - \frac{E_2 h^3}{12(1-\nu_{12}\nu_{21})} \frac{\phi_2}{r} \right) - k G_{23} h \left(\frac{\partial w_2}{\partial r} + \phi_2 \right) = 0 \quad (20)$$

Then, the governing equations on the basis of the adjacent equilibrium method are transformed to the linear stability equations as follows:

$$k_0 (w_1 - w_2) + N_\theta^{th} \left(\frac{-\mu + r^2}{r^3} \frac{\partial w_1}{\partial r} + \frac{\mu}{r^2} \frac{\partial^2 w_1}{\partial r^2} - \frac{\mu}{r} \frac{\partial^3 w_1}{\partial r^3} \right) + N_r^{th} \left(\frac{\partial^2 w_1}{\partial r^2} - \mu \frac{\partial^4 w_1}{\partial r^4} - \frac{\mu}{r} \frac{\partial^3 w_1}{\partial r^3} \right) - k_0 \mu \left(\frac{\partial^2 w_1}{\partial r^2} + \frac{1}{r} \frac{\partial w_1}{\partial r} - \frac{\partial^2 w_2}{\partial r^2} - \frac{1}{r} \frac{\partial w_2}{\partial r} \right) + k G_{23} h \left(\frac{\partial^2 w_1}{\partial r^2} + \frac{\partial \phi_1}{\partial r} \right) + k G_{23} h \frac{1}{r} \left(\frac{\partial w_1}{\partial r} + \phi_1 \right) = 0 \quad (21)$$

$$k_0 (w_2 - w_1) - k_w w_2 + k_p \left(\frac{\partial^2 w_2}{\partial r^2} + \frac{1}{r} \frac{\partial w_2}{\partial r} \right) - k_0 \mu \left(\frac{\partial^2 w_2}{\partial r^2} - \frac{\partial^2 w_1}{\partial r^2} + \frac{1}{r} \frac{\partial w_2}{\partial r} - \frac{1}{r} \frac{\partial w_1}{\partial r} \right) + k_w \mu \left(\frac{\partial^2 w_2}{\partial r^2} + \frac{1}{r} \frac{\partial w_2}{\partial r} \right) - k_p \mu \left(\frac{\partial^4 w_2}{\partial r^4} + \frac{2}{r} \frac{\partial^3 w_2}{\partial r^3} - \frac{1}{r^2} \frac{\partial^2 w_2}{\partial r^2} + \frac{1}{r^3} \frac{\partial w_2}{\partial r} \right) + N_\theta^{th} \left(\frac{-\mu + r^2}{r^3} \frac{\partial w_2}{\partial r} + \frac{\mu}{r^2} \frac{\partial^2 w_2}{\partial r^2} - \frac{\mu}{r} \frac{\partial^3 w_2}{\partial r^3} \right) + N_r^{th} \left(\frac{\partial^2 w_2}{\partial r^2} - \mu \frac{\partial^4 w_2}{\partial r^4} - \frac{\mu}{r} \frac{\partial^3 w_2}{\partial r^3} \right) + k G_{23} h \left(\frac{\partial^2 w_2}{\partial r^2} + \frac{\partial \phi_2}{\partial r} \right) + \frac{1}{r} k G_{23} h \left(\frac{\partial w_2}{\partial r} + \phi_2 \right) = 0 \quad (22)$$

in which the thermal stress resultants along the radius and angle of the circular plate can be presented as below:

$$N_r^{th} = \frac{E_1 \alpha_1 h}{(1-\nu_{12}\nu_{21})} \Delta T + \frac{E_1 \nu_{21} \alpha_2 h}{(1-\nu_{12}\nu_{21})} \Delta T \quad (23)$$

$$N_\theta^{th} = \frac{E_2 \alpha_2 h}{(1-\nu_{12}\nu_{21})} \Delta T + \frac{E_1 \nu_{21} \alpha_1 h}{(1-\nu_{12}\nu_{21})} \Delta T \quad (24)$$

where ΔT is the linear change in the temperature as $\Delta T = T_2 - T_1$ (T_1 denotes the room temperature as 300 Kelvin and T_2 represents the final temperature which makes the plate in a buckled form). In this paper, the increase in temperature is assumed to be linear and the temperature along the thickness is constant. Other parameters respectively, α_1 and α_2 are the thermal expansion coefficients for the orthotropic plate, and the other ones are the elastic properties as defined before.

3. Solution Process

In this paper, the differential quadrature method (DQM) is employed in order to solve the equilibrium equations. This



method has proven to provide excellent accuracy, efficiency, convenience, and great potential in solving complicated partial differential equations [51]. Therefore, the DQM, as well as simple formulation, provides low computational cost unlike other numerical methods such as dynamic relaxation method (DRM), finite difference method (FDM), finite element method (FEM), and etc. The DQM was introduced by Bellman and Casti [82-83]. Many researchers have recently advocated the application of the DQM for the investigation of nanostructures [84-87]. The basic idea of the DQM is based on the approximation of partial derivative of a function with respect to a space variable at a discrete point as a weighted linear sum of the function values at all discrete points in the whole domain. Its weighting coefficients alone depend on the grid spacing. Therefore, every partial differential equation can be converted into a number of algebraic equations using these coefficients [64]. DQM can be subdivided into several subsets the applied function and satisfying types of boundary conditions. In this paper, polynomial function and direct substitution techniques are utilized for this purpose. By using the DQM, derivatives of a function f_r at point r_i is defined by:

$$\left. \frac{d^{(n)} f}{dr} \right|_{r_i} = \sum_{k=1}^N a_{ik}^{(n)} f(r_k) \quad i = 1, \dots, N \tag{25}$$

$$A_{ij}^{(n)} = n \left[A_{ij}^1 A_{ii}^{(n-1)} - \frac{A_{ij}^{(n-1)}}{(r_i - r_j)} \right] \quad i \neq j \tag{26}$$

$$A_{ii}^{(n)} = - \sum_{j=1, \neq i}^N A_{ij}^{(n)} \quad i, j = 1 \dots N \tag{27}$$

in which, N is the number of grid points along r direction. It is more offered to use the grid point distribution which is based on Chebyshev-Gauss-Lobatto points to gain more accurate results [64]. According to the Chebyshev-Gauss-Lobatto grid point's distribution, the coordinates of the grid points are as follows:

$$r_i = \left(\frac{r}{2} - \cos \left(\left(\frac{i-1}{N-1} \right) \pi \right) \right) \left(\frac{r}{2} \right), \quad i = 1, \dots, N \tag{28}$$

With the implementation of DQM into the Eqs. (21) and (22), the following equations can be obtained:

$$\begin{aligned} & k_0 (w_1^1 - w_2^1) + \left(\frac{E_2 \alpha_{22} h}{(1 - \nu_{12} \nu_{21})} \Delta T \left(-\frac{\mu + r^2}{r^3} \sum_{k=1}^N C_{ik} w_{1kj}^1 + \frac{\mu}{r^2} \sum_{k=1}^N C_{ik}^2 w_{1kj}^1 - \frac{\mu}{r} \sum_{k=1}^N C_{ik}^3 w_{1kj}^1 \right) \right) \\ & + \left(\frac{E_1 \alpha_{11} h}{(1 - \nu_{12} \nu_{21})} \Delta T \left(\sum_{k=1}^N C_{ik}^2 w_{1kj}^1 - \mu \sum_{k=1}^N C_{ik}^4 w_{1kj}^1 - \frac{\mu}{r} \sum_{k=1}^N C_{ik}^3 w_{1kj}^1 \right) \right) \\ & - k_0 \mu \left(\sum_{k=1}^N C_{ik}^2 w_{1kj}^1 + \frac{1}{r} \sum_{k=1}^N C_{ik} w_{1kj}^1 - \sum_{k=1}^N C_{ik}^2 w_{2kj}^1 - \frac{1}{r} \sum_{k=1}^N C_{ik} w_{2kj}^1 \right) \\ & + k G_{23} h \left(\sum_{k=1}^N C_{ik}^2 w_{1kj}^1 + \sum_{k=1}^N C_{ik} \phi_{1kj}^1 \right) + k G_{23} h \frac{1}{r} \left(\sum_{k=1}^N C_{ik} w_{1kj}^1 + \phi^1 \right) = 0 \end{aligned} \tag{29}$$

$$\begin{aligned} & k_0 (w_2^1 - w_1^1) - k_w w_2^1 + k_p \left(\sum_{k=1}^N C_{ik}^2 w_{2kj}^1 + \frac{1}{r} \sum_{k=1}^N C_{ik} w_{2kj}^1 \right) - k_0 \mu \left(\sum_{k=1}^N C_{ik}^2 w_{2kj}^1 - \sum_{k=1}^N C_{ik}^2 w_{1kj}^1 + \frac{1}{r} \sum_{k=1}^N C_{ik} w_{2kj}^1 - \frac{1}{r} \sum_{k=1}^N C_{ik} w_{1kj}^1 \right) \\ & + k_w \mu \left(\sum_{k=1}^N C_{ik}^2 w_{2kj}^1 + \frac{1}{r} \sum_{k=1}^N C_{ik} w_{2kj}^1 \right) - k_p \mu \left(\sum_{k=1}^N C_{ik}^4 w_{2kj}^1 + \frac{2}{r} \sum_{k=1}^N C_{ik}^3 w_{2kj}^1 - \frac{1}{r^2} \sum_{k=1}^N C_{ik}^2 w_{2kj}^1 + \frac{1}{r^3} \sum_{k=1}^N C_{ik} w_{2kj}^1 \right) \\ & + \left(\frac{E_2 \alpha_{22} h}{(1 - \nu_{12} \nu_{21})} \Delta T \left(-\frac{\mu + r^2}{r^3} \sum_{k=1}^N C_{ik} w_{1kj}^1 + \frac{\mu}{r^2} \sum_{k=1}^N C_{ik}^2 w_{1kj}^1 - \frac{\mu}{r} \sum_{k=1}^N C_{ik}^3 w_{1kj}^1 \right) \right) \\ & + \left(\frac{E_1 \alpha_{11} h}{(1 - \nu_{12} \nu_{21})} \Delta T \left(\sum_{k=1}^N C_{ik}^2 w_{2kj}^1 - \mu \sum_{k=1}^N C_{ik}^4 w_{2kj}^1 - \frac{\mu}{r} \sum_{k=1}^N C_{ik}^3 w_{2kj}^1 \right) \right) \\ & + k G_{23} h \left(\sum_{k=1}^N C_{ik}^2 w_{2kj}^1 + \sum_{k=1}^N C_{ik} \phi_{2kj}^1 \right) + \frac{1}{r} k G_{23} h \left(\sum_{k=1}^N C_{ik} w_{2kj}^1 + \phi^1 \right) = 0 \end{aligned} \tag{30}$$

Here, the obtained equations are converted into a dimensionless schema using the following relations:

$$A_{11} = \frac{E_1 h}{(1 - \nu_{12} \nu_{21})} ; \quad A_{22} = \frac{E_2 h}{(1 - \nu_{12} \nu_{21})} ; \quad A_{12} = \frac{\nu_{21} E_1 h}{(1 - \nu_{12} \nu_{21})} \tag{31}$$

$$A_{55} = kG_{23}h ; D_{11} = \frac{E_1 h^3}{12(1-\nu_{12}\nu_{21})} ; D_{22} = \frac{E_2 h^3}{12(1-\nu_{12}\nu_{21})} ; D_{12} = \nu_{12}D_{22}$$

$$\gamma_0 = \frac{k_0 r_0^2}{A_{55}} ; \gamma_1 = \frac{k_w r_0^2}{A_{55}} ; \gamma_2 = \frac{k_p}{A_{55}} ; \lambda_1 = \frac{D_{11}}{A_{55} r_0^2} ; \lambda_2 = \frac{D_{22}}{A_{55} r_0^2} ; \lambda_3 = \frac{D_{12}}{A_{55} r_0^2}$$

$$A_1 T = [A_{11} A_{12}] [\alpha_1 ; \alpha_2] ; A_2 T = [A_{12} A_{22}] [\alpha_1 ; \alpha_2] ; \lambda_4 = \frac{A_1 T}{A_{55} \alpha_1} ; \lambda_5 = \frac{A_2 T}{A_{55} \alpha_1}$$

$$\xi = \frac{\mu}{r_0^2} ; R = \frac{r}{r_0} ; W = \frac{w}{r_0} ; T^* = 10^4 \Delta T \alpha_1 ; \Phi = \phi$$

Finally, in order to solve the Eqs. (29) and (30), the boundary conditions should be defined.

1- Simply-supported boundary conditions (S):

$$w = M_r = 0 \quad (32)$$

2- Clamped boundary conditions (C):

$$w = \phi = 0 \quad (33)$$

4. Results and Discussions

To validate the outcomes of the present research, Ref. [59] is employed in which the dimensionless strain at the buckling time was analyzed for a circular isotropic SLGS with clamped boundary conditions. In this reference, the classical plate theory was also applied.

$$\varepsilon_b = \frac{14.6819h^2}{12(R^2 + 14.6189(e_0 a)^2)(1-\nu^2)}, \quad \nu = 0.3, \quad h = 0.335nm \quad (34)$$

Table 1. Comparison of the nondimensional strain at the buckling time of circular SLGS with clamped boundary conditions

Reference	r (nm)	The percent of the strain of buckling (ε_b (%))				
		$e_0 a$ (nm)				
		0	0.5	1	1.5	2
Present work	4	0.9205	0.7487	0.4800	0.3003	0.1968
Ref. [59]		0.9430	0.7671	0.4918	0.3077	0.2019
Present work	6	0.4146	0.3763	0.2945	0.2162	0.1576
Ref. [59]		0.4191	0.3803	0.2977	0.2186	0.1593
Present work	8	0.2343	0.2216	0.1906	0.1546	0.1222
Ref. [59]		0.2358	0.2230	0.1918	0.1555	0.1229
Present work	10	0.1503	0.1450	0.1311	0.1130	0.0947
Ref. [59]		0.1509	0.1455	0.1316	0.1134	0.0951

Table 2. Comparison of the nondimensional strain at the buckling time of circular SLGS and BLGS with clamped boundary conditions

Reference	r (nm)	The percent of the strain of buckling (ε_b (%))				
		$e_0 a$ (nm)				
		0	0.5	1	1.5	2
Present work-SLGS	4	0.9205	0.7487	0.4800	0.3003	0.1968
Present work-BLGS		1.3871	1.1945	0.8575	0.4938	0.3434
[SL]	6	0.4146	0.3763	0.2945	0.2162	0.1576
[BL]		1.2454	1.1286	0.8480	0.5501	0.3989
[SL]	8	0.2343	0.2216	0.1906	0.1546	0.1222
[BL]		1.1160	1.0196	0.8283	0.5744	0.4330
[SL]	10	0.1503	0.1450	0.1311	0.1130	0.0947
[BL]		1.0499	0.9899	0.8189	0.5926	0.4658

As it is found from Table 1, the percent of strain at the mechanical buckling for various nonlocal parameters and several radii are in good agreement with the literature. On the other hand, by Table 2, a comparison study is displayed for percent of dimensionless strain at the time of buckling between SLGS and BLGS whilst the edge conditions are clamped ones.

In this paper, thermal buckling of the orthotropic circular BLGS embedded in an elastic matrix is investigated based on nonlocal first-order shear deformation theory and von Kármán nonlinear strains. Mechanical properties of graphene sheets are dependent on some components such as atoms chirality and dimensions of the sheet [76]. Moreover, the hexagonal arrangement of Carbon's atoms leads to different angles between C–C bonds with in-plane loads for different directions [61]. Thus, as mentioned it has been reported that the mechanical properties of a graphene sheet are anisotropic so that the difference between elastic modulus of a graphene sheet along the different directions is related to inter-atomic bond orientation. Therefore, for the precise prediction of the thermal behaviors of a circular nanoplate resting on two parameters elastic foundation the following orthotropic material properties and nondimensional definitions are used in this study, unless stated otherwise.

$$E_1 = 1765GPa, E_2 = 1584GPa, \nu_{12} = 0.3, \nu_{21} = 0.25, r = 5nm, \alpha_1 = 1.1 \times 10^{-6} \tag{35}$$

$$h = 0.335nm, k_w = 2GPa / nm, k_p = 2Pa.m, C = 45GPa / nm, e_0 a = 1nm$$

Figures (2) and (3) represent the effects of the radius of the nanoplate on the critical buckling temperature for various nonlocal parameters for clamped and simply-supported boundary conditions, respectively. It can be observed that whatever the nonlocal parameter increases the critical temperature would be decreased. In addition to this, by the increase of the radius and nonlocal parameter, the obtained critical temperatures are reaching each other. It should be noted that this trend for simply-supported boundary conditions is more visible than clamped ones. Moreover, at a radius of 14.9 nm, the difference between nonlocal and local cases at a nonlocal parameter value of 2 nm is in the greatest value and this difference decreases by an increase in radius from 14.9 to 74.6. It can be seen that for simply-supported boundary conditions, by the increase of radius and nonlocal parameter from 0 to 1 the critical temperature initially decreases and then increases. But, at values of 1.5 and 2 nm, by the increase of the radius, the critical temperature has been raised with a gentle slope in a continuous trend for both simple and clamped boundary conditions. Also, at clamped boundary conditions by an increase in radius, the difference between nonlocal and local analyses decreases compared to simply-supported boundary conditions. Furthermore, the difference percent of critical temperature at nonlocal values of 1.5 and 2 nm and also at the amplitude of radius from 14.9 to 74.6 for the simple boundary is further than clamped one.

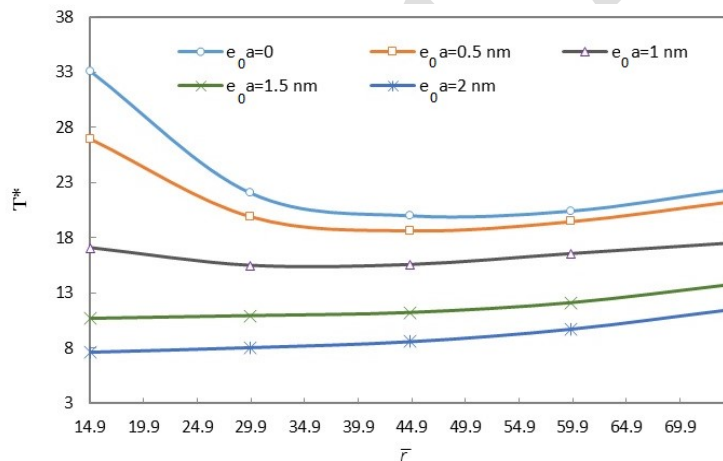


Fig. 2. The variations of thermal buckling load in terms of dimensionless radius and several nonlocal parameters for clamped boundary conditions

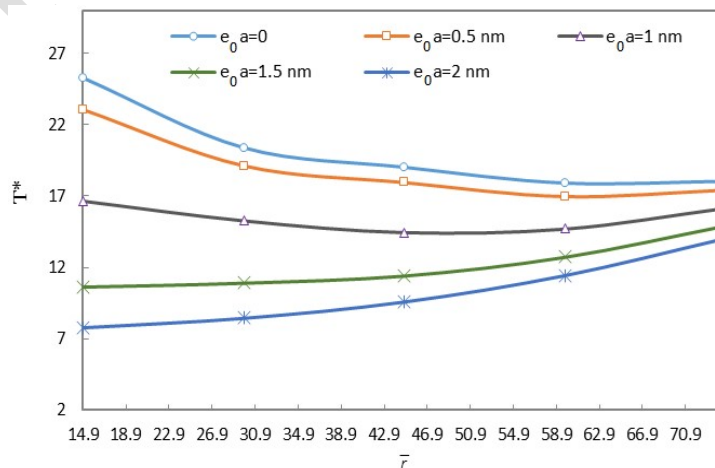


Fig. 3. The variations of thermal buckling load in terms of dimensionless radius and several nonlocal parameters for simple boundary conditions

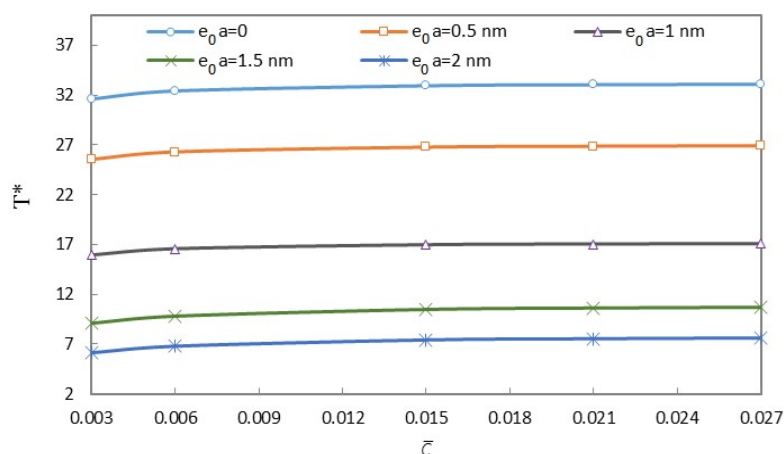


Fig. 4. The variations of thermal buckling load in terms of dimensionless vdW coefficient and several nonlocal parameters for clamped boundary conditions

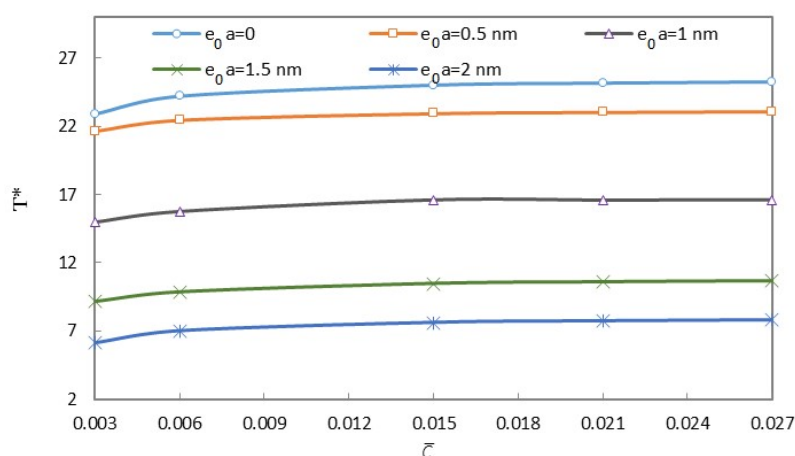


Fig. 5. The variations of thermal buckling load in terms of dimensionless vdW coefficient and several nonlocal parameters for simply-supported boundary conditions

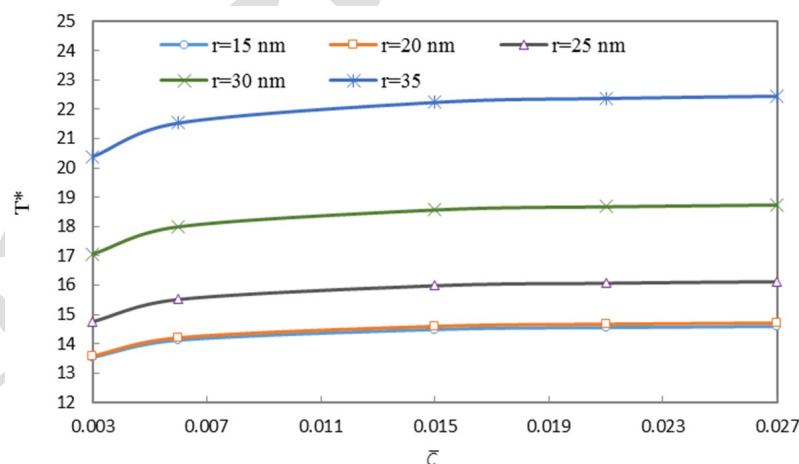


Fig. 6. The variations of thermal buckling load in terms of dimensionless vdW coefficient and different radiuses for simply-supported boundary conditions

Figures (4) and (5) exhibit the effect of variations of the vdW coefficient on the critical temperature with several nonlocal parameters for clamped and simply-supported boundary conditions, respectively. As can be seen, whatever the nonlocal parameter is increased the critical temperature is decreased. As it is found, the difference between nonlocal and local results whilst $e_0a=0.5$ nm for the pivot boundary is less than clamped one and the increase of vdW forces does not affect considerably this difference. Furthermore, by increasing the vdW from 0.003 to 0.027, the critical temperature of buckling has not remarkable changes and this behavior can be seen at all boundary conditions.

The impacts of variations of the vdW forces on the critical temperature of buckling for different radiuses have been plotted and exhibited in Fig. (6) and (7) for simply-supported and clamped boundary conditions, respectively. It can be

seen that for the simple boundary, the change in radius of 15 to 20 nm does not affect considerably the critical temperature. Moreover, the value of the difference in the critical temperature of buckling for both boundary conditions in the radius of 15 to 20 nm is less than the difference in the critical temperature of buckling in the radius of 25 nm to upward. Therefore, the variations of vdW do not impress this trend. From Figs. (6) and (7), it can also be concluded that the increasing percentage of the slope which originated from variations of vdW, in the initial values of this parameter is much more than its larger values. So that for a coefficient of vdW with a value of 0.015 up to the next, it can be stated that the slopes of the curves are almost zero and change in boundary conditions and radius of nanoplate does not create a variation in this process. This means that after this value of vdW, both nanoplates are converted into an SLGs model.

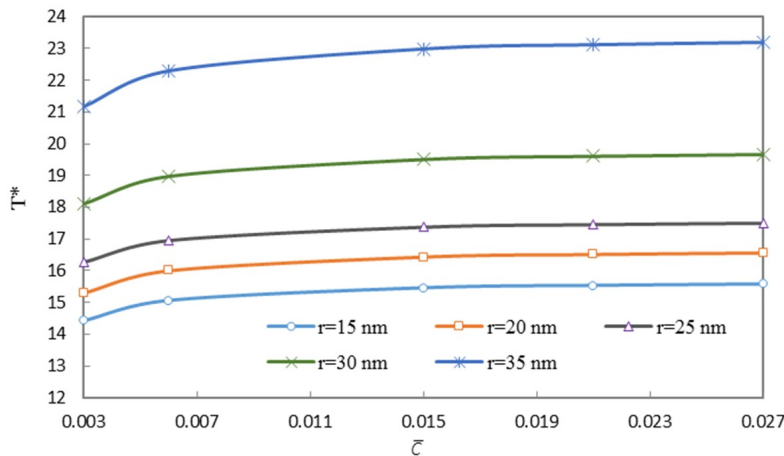


Fig. 7. The variations of thermal buckling load in terms of dimensionless vdW coefficient and different radiuses for clamped boundary conditions

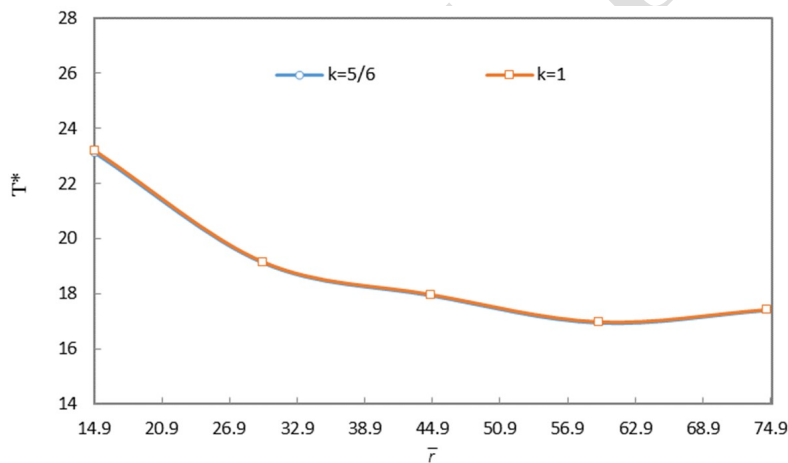


Fig. 8. The variations of thermal buckling load in terms of shear correction factor and different dimensionless radiuses for simply-supported boundary conditions

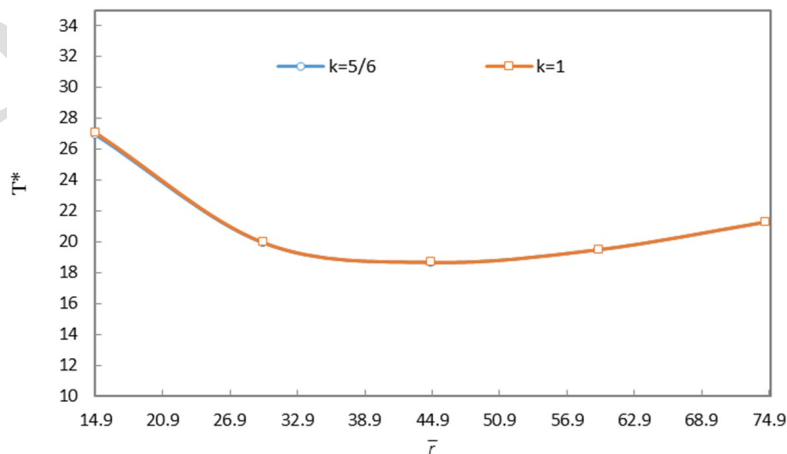


Fig. 9. The variations of thermal buckling load in terms of shear correction factor and different dimensionless radiuses for clamped boundary conditions

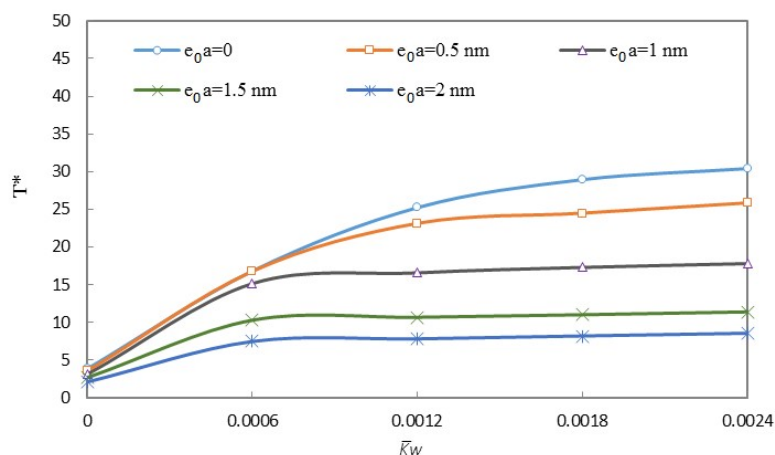


Fig. 10. The variations of thermal buckling load in terms of dimensionless Winkler coefficient and different nonlocal parameter for simply-supported boundary conditions

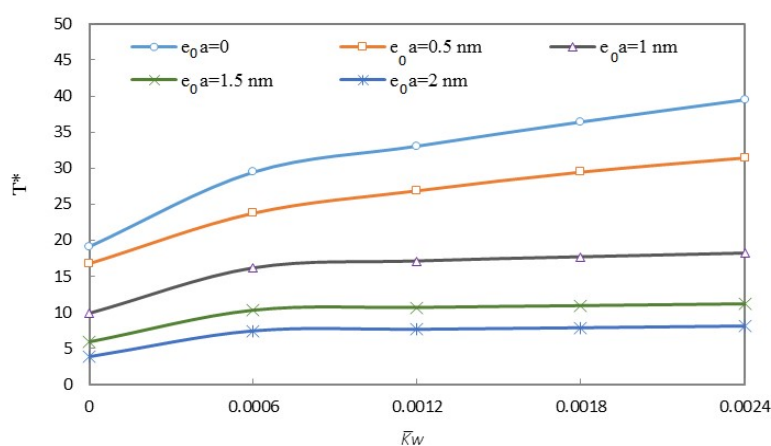


Fig. 11. The variations of thermal buckling load in terms of dimensionless Winkler coefficient and different nonlocal parameter for clamped boundary conditions

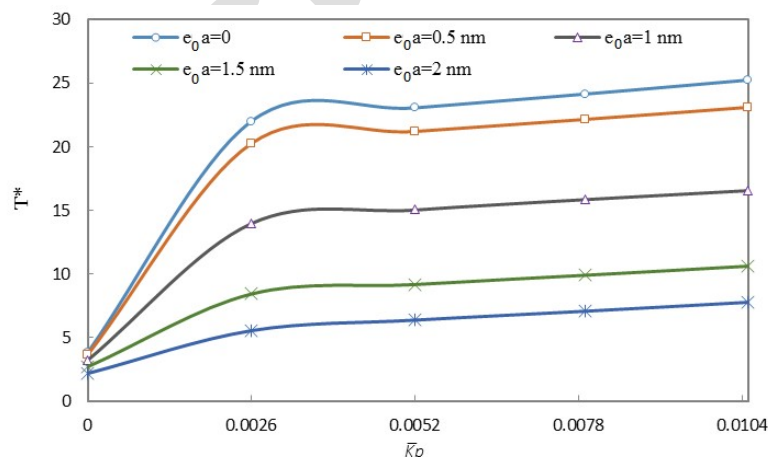


Fig. 12. The variations of thermal buckling load in terms of dimensionless Pasternak shear coefficient and different nonlocal parameter for simply-supported boundary conditions

The influences of changes in the radius on the critical temperature of buckling for various shear correction factors for simply-supported and clamped boundary conditions are shown by Figs. (8) and (9), respectively. As can be seen, in these problems, the variations in the shear correction factor from $k=5/6$ to $k=1$ do not affect the response and for both boundary conditions, this can be proved. It is interesting to note that in the clamped conditions with enlarging of non-dimensional radius up to 44.9, the critical temperature is reduced and for values of greater than 44.9, the critical temperature would be increased. However, the changes of non-dimensional radius from 14.9 to 74.9 do not affect this trend for simply supported boundary conditions. With a comparison of both Figs. (8) and (9), this conclusion would be found that the difference percent in the critical temperature of buckling, by varying the non-dimensional radius from 14.9 to 74.9, is more significant in clamped boundary conditions compared to the simply-supported ones.

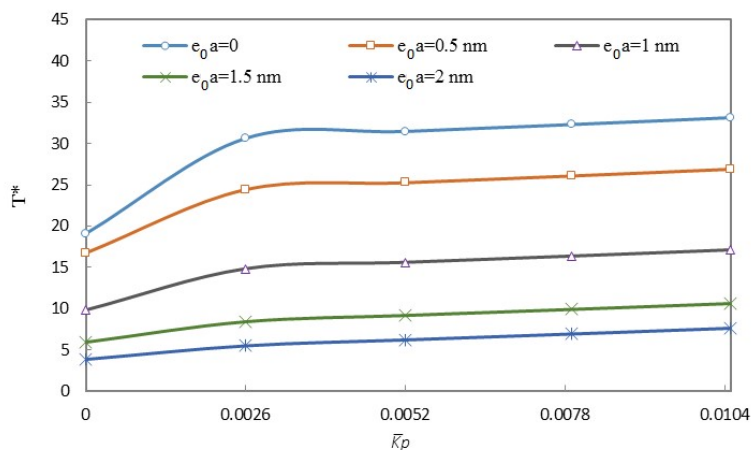


Fig. 13. The variations of thermal buckling load in terms of dimensionless Pasternak shear coefficient and different nonlocal parameter for clamped boundary conditions

The Figs. (10) and (11) demonstrate the effects of Winkler coefficient of the elastic foundation on the critical temperature of buckling in different nonlocal and local cases for simply-supported and clamped boundary conditions, respectively. As it is shown, whenever the nonlocal parameter is greater, the slope of the curves decreased. Furthermore, for simply-supported boundary conditions unlike the clamped ones, in the case that the elastic foundation is removed, the variations of nonlocal parameter do not affect remarkably the critical temperature. Also, with regards to the Figs. (10) and (11), it can be found that the elastic foundation does not affect significantly the critical temperature of buckling. However, with increasing the Winkler parameter the critical temperature increased. It is worth mentioning that the slope of this increasing trend for the initial values of the Winkler parameter is more than the larger values of this parameter. In addition, at simply-supported boundary conditions for the values of the Winkler elastic foundation till 0.0006, the results of nonlocal and local cases until the $e_0 a = 1$ nm are approximately identical. Hence, it can be stated that in these conditions there is no need to analyze nonlocality and the simple local analysis is enough. This conclusion cannot be found for clamped boundary conditions like simply-supported ones. Moreover, by comparing Figs. (10) and (11), it is illustrated that the difference percent of deflection resulted from an increase in Winkler parameter from 0 to 0.0024 for the simply-supported boundary condition is more than the clamped one.

Figures (12) and (13) show the effects of variations of Pasternak medium on the critical buckling temperature for several nonlocal and local cases for simply-supported and clamped boundaries, respectively. It can be observed that with the increase in the stiffness value of the Pasternak matrix and nonlocal parameter, the critical temperature increased for both boundary conditions. Furthermore, for simply-supported boundary conditions unlike clamped ones, in the system without any foundation, the changes in nonlocal parameter do not affect remarkably the critical buckling temperature.

5. Conclusion

In this research, the thermal buckling behavior of circular bilayer orthotropic nanoplates was presented. As far as the modeled plate is a size-dependent one, to apply the influences of small scale behavior, the nonlocal elasticity theory of Eringen was used. The nonlinear equilibrium equations were derived using the energy formulation based on the first-order shear deformation theory and nonlinear strains of von Kármán. The critical buckling temperature was obtained by utilizing the equilibrium adjacent method that is a method for linearizing the nonlinear equations. These equations were discretized based on the differential quadrature method for simply-supported and clamped boundary conditions. Then, by solving the determinant of the matrix of coefficients of the algebraic linear equations system, the critical buckling temperature was calculated. In order to verify and validate the results of the present work, the outcomes were compared with other papers. Finally, some effective parameters such as nonlocal factor, the ratio of thickness-to-radius, the temperature of the environment, boundary conditions, thickness of the nanoplate and impacts of the elastic matrix on the critical buckling temperatures were considered in which the following notable points are abbreviated:

- By increase of the radius, the critical temperature would be raised and with an increase in the small scale factor, the critical temperature decreased. Also, whatever the boundary conditions are flexible, the variations of critical temperatures are smaller.
- The percent of changes in the critical temperature of buckling on the basis of vdW variations is more at lower vdW coefficients compared to the higher vdW ones.
- For simply-supported boundary conditions, unlike the clamped ones, for the case that the elastic matrix does not exist, the variations of the nonlocal parameter do not affect the critical temperature.

Author Contributions

Author 1 planned the scheme, initiated the project and suggested the experiments; Author 2 conducted the

experiments and analyzed the empirical results; Author 3 developed the mathematical modeling and examined the theory validation. The manuscript was written through the contribution of all authors. All authors discussed the results, reviewed and approved the final version of the manuscript.

Conflict of Interest

The authors declared no potential conflicts of interest with respect to the research, authorship, and publication of this article.

Funding

The authors received no financial support for the research, authorship and publication of this article.

References


- [1] Drexler, K.E., Nanosystems: molecular machinery, manufacturing, and computation, John Wiley & Sons, 1992.
- [2] Li, M., Tang, H.X., Roukes, M.L., Ultra-sensitive NEMS-based cantilevers for sensing, scanned probe and very high-frequency applications, *Nature Nanotechnology*, 2, 2007, 114–33.
- [3] Cimalla, V., Niebelschütz, F., Tonisch, K., Foerster, Ch., Brueckner, K., Cimalla, I., et al., Nanoelectromechanical devices for sensing applications, *Sensors and Actuators B: Chemical*, 126, 2007, 24–34.
- [4] Sakhaee-Pour, A., Ahmadian, M.T., Vafai, A., Applications of single-layered graphene sheets as mass sensors and atomistic dust detectors, *Solid State Communications*, 145, 2008, 168–72.
- [5] Wang, J., Li, Z., Fan, G., Pan, H., Chen, Z., Zhang, D., Reinforcement with graphene nanosheets in aluminum matrix composites, *Scripta Materialia*, 66, 2012, 594–7.
- [6] Iijima, S., Helical microtubules of graphitic carbon, *Nature*, 354, 1991, 56–63.
- [7] Lu, B.P., Zhang, P.Q., Lee, H.P., Wang, C.M., Reddy, J.N., Non-local elastic plate theories, *Proceedings of the Royal Society*, A 463, 2007, 3225–40.
- [8] Reddy, J.N., Microstructure-dependent couple stress theories of functionally graded beams, *Journal of the Mechanics and Physics of Solids*, 59, 2011, 2382–99.
- [9] Akgöz, B., Civalek, Ö., A size-dependent shear deformation beam model based on the strain gradient elasticity theory, *International Journal of Engineering Science*, 70, 2013, 1–14.
- [10] Akgöz, B., Civalek, Ö., Buckling analysis of functionally graded microbeams based on the strain gradient theory, *Acta Mechanica*, 224, 2013, 2185–201.
- [11] Lam, D.C.C., Yang, F., Chong, A.C.M., Wang, J., Tong, P., Experiments and theory in strain gradient elasticity, *Journal of the Mechanics and Physics of Solids*, 51, 2003, 1477–508.
- [12] Akgöz, B., Civalek, Ö., Analysis of micro-sized beams for various boundary conditions based on the strain gradient elasticity theory, *Archive of Applied Mechanics*, 82, 2012, 423–443.
- [13] Ke, L.L., Wang, Y.S., Yang, J., Kitipornchai, S., Free vibration of size-dependent Mindlin microplates based on the modified couple stress theory, *Journal of Sound and Vibration*, 331, 2012, 94–106.
- [14] Akgöz, B., Civalek, Ö., Strain gradient elasticity, and modified couple stress models for buckling analysis of axially loaded micro-scaled beams, *International Journal of Engineering Science*, 49, 2011, 1268–80.
- [15] Akgöz, B., Civalek, Ö., Buckling analysis of cantilever carbon nanotubes using the strain gradient elasticity and modified couple stress theories, *Journal of Computational and Theoretical Nanoscience*, 8, 2011, 1821–1827.
- [16] Akgöz, B., Civalek, Ö., Free vibration analysis of axially functionally graded tapered Bernoulli–Euler microbeams based on the modified couple stress theory, *Composite Structures*, 98, 2013, 314–22.
- [17] Akgöz, B., Civalek, Ö., Modeling, and analysis of micro-sized plates resting on elastic medium using the modified couple stress theory, *Meccanica*, 48, 2013, 863–873.
- [18] Yang, F., Chong, A.C.M., Lam, D.C.C., Tong, P., Couple stress based strain gradient theory for elasticity, *International Journal of Solids Structures*, 39, 2002, 2731–43.
- [19] Malikan, M., Electro-mechanical shear buckling of piezoelectric nanoplate using modified couple stress theory based on simplified first-order shear deformation theory, *Applied Mathematical Modelling*, 48, 2017, 196–207.
- [20] Malikan, M., Analytical predictions for the buckling of a nanoplate subjected to non-uniform compression based on the four-variable plate theory, *Journal of Applied and Computational Mechanics*, 3, 2017, 218–228.
- [21] Malikan, M., Buckling analysis of a micro composite plate with nano-coating based on the modified couple stress theory, *Journal of Applied and Computational Mechanics*, 4, 2018, 1–15.
- [22] Malikan, M., Temperature influences on shear stability of a nanosize plate with piezoelectricity effect, *Multidiscipline Modeling in Materials and Structures*, 14, 2018, 125–142.
- [23] Malikan, M., Electro-thermal buckling of elastically supported double-layered piezoelectric nanoplates affected by an external electric voltage, *Multidiscipline Modeling in Materials and Structures*, 15, 2019, 50–78.
- [24] Eringen, A.C., Edelen, D.G.B., On nonlocal elasticity, *International Journal of Engineering Science*, 10, 1972, 233–48.
- [25] Eringen, A.C., On differential equations of nonlocal elasticity, solutions of screw dislocation, surface waves, *Journal of Applied Physics*, 54, 1983, 4703–10.


- [26] Eringen, A.C., *Nonlocal continuum field theories*, New York, Springer, 2002.
- [27] Eringen, A.C., Nonlocal continuum mechanics based on distributions, *International Journal of Engineering Science*, 44, 2006, 141-7.
- [28] Malikan, M., Jabbarzadeh, M., Dastjerdi, Sh., Non-linear Static stability of bi-layer carbon nanosheets resting on an elastic matrix under various types of in-plane shearing loads in thermo-elasticity using nonlocal continuum, *Microsystem Technologies*, 23, 2017, 2973–2991.
- [29] Malikan, M., Nguyen, V.B., A novel one-variable first-order shear deformation theory for biaxial buckling of a size-dependent plate based on the Eringen's nonlocal differential law, *World Journal of Engineering*, 15, 2018, 633-645.
- [30] Malikan, M., On the buckling response of axially pressurized nanotubes based on a novel nonlocal beam theory, *Journal of Applied and Computational Mechanics*, 5, 2019, 103-112.
- [31] Malikan, M., Tornabene, F., Dimitri, R., Nonlocal three-dimensional theory of elasticity for buckling behavior of functionally graded porous nanoplates using volume integrals, *Materials Research Express*, 5, 2018, 095006.
- [32] Golmakani, M.E., Malikan, M., Sadraee Far, M.N., Majidi, H.R., Bending and buckling formulation of graphene sheets based on nonlocal simple first-order shear deformation theory, *Materials Research Express*, 5, 2018, 065010.
- [33] Malikan, M., Sadraee Far, M.N., Differential quadrature method for dynamic buckling of graphene sheet coupled by a viscoelastic medium using neperian frequency based on nonlocal elasticity theory, *Journal of Applied and Computational Mechanics*, 4, 2018, 147-160.
- [34] Sadraee Far, M.N., Golmakani, M.E., Large deflection of thermo-mechanical loaded bilayer orthotropic graphene sheet in/on polymer matrix based on nonlocal elasticity theory, *Computers and Mathematics with Applications*, 76, 2018, 2061-89.
- [35] Ansari, R., Torabi, J., Nonlocal vibration analysis of circular double-layered graphene sheets resting on an elastic foundation subjected to thermal loading, *Acta Mechanica Sinica*, 32, 2016, 841-853.
- [36] Dastjerdi, Sh., Akgöz, B., Yazdanparast, L., A new approach for bending analysis of bilayer conical graphene panels considering nonlinear van der Waals force, *Composites Part B: Engineering*, 150, 2018, 124-134.
- [37] Demir, C., Civalek, Ö., Torsional and longitudinal frequency and wave response of microtubules based on the nonlocal continuum and nonlocal discrete models, *Applied Mathematical Modelling*, 37, 2013, 9355-9367.
- [38] Pradhan, S.C., Kumar, A., Vibration analysis of orthotropic graphene sheets using nonlocal elasticity theory and differential quadrature method, *Composite Structures*, 93, 2011, 774-779.
- [39] Prasanna, T.J., Kumar, S., Gopalakrishnan, N.S., Thermal vibration analysis of monolayer graphene embedded in elastic medium based on nonlocal continuum mechanics, *Composite Structures*, 100, 2013, 332-342.
- [40] Numanoglu, H.M., Akgöz, B., Civalek, Ö., On dynamic analysis of nanorods, *International Journal of Engineering Science*, 130, 2018, 33-50.
- [41] She, G.L., Yuan, F.G., Ren, Y.R., Xiao, W.Sh., On buckling and post-buckling behavior of nanotubes, *International Journal of Engineering Science*, 121, 2018, 130–142.
- [42] Malikan, M., Nguyen, V.B., Buckling analysis of piezo-magnetoelectric nanoplates in a hygrothermal environment based on a novel one variable plate theory combining with higher-order nonlocal strain gradient theory, *Physica E: Low-dimensional Systems and Nanostructures*, 102, 2018, 8-28.
- [43] Malikan, M., Nguyen, V.B., Tornabene, F., Electromagnetic forced vibrations of composite nanoplates using nonlocal strain gradient theory, *Materials Research Express*, 5, 2018, 075031.
- [44] Malikan, M., Nguyen, V.B., Tornabene, F., Damped forced vibration analysis of single-walled carbon nanotubes resting on viscoelastic foundation in thermal environment using nonlocal strain gradient theory, *Engineering Science and Technology, an International Journal*, 21, 2018, 778-786.
- [45] Malikan, M., Dimitri, R., Tornabene, F., Effect of Sinusoidal Corrugated Geometries on the Vibrational response of Viscoelastic Nanoplates, *Applied Sciences*, 8, 2018, 1432.
- [46] Malikan, M., Nguyen, V.B., Dimitri, R., Tornabene, F., Dynamic modeling of non-cylindrical curved viscoelastic single-walled carbon nanotubes based on the second gradient theory, *Materials Research Express*, 6, 2019, 075041.
- [47] Malikan, M., Dimitri, R., Tornabene, F., Transient response of oscillated carbon nanotubes with internal and external damping, *Composites Part B Engineering*, 158, 2019, 198-205.
- [48] She, G.L., Yuan, F.G., Ren, Y.R., Liu, H.B., Xiao, W.Sh., Nonlinear bending and vibration analysis of functionally graded porous tubes via a nonlocal strain gradient theory, *Composite Structures*, 203, 2018, 614–23.
- [49] Shen, L., Shen, H.S., Zhang, C.L., Nonlocal plate model for nonlinear vibration of single-layer graphene sheets in thermal environments, *Computational Materials Science*, 48, 2010, 680–5.
- [50] Pradhan, S.C., Kumar, A., Vibration analysis of orthotropic graphene sheets embedded in Pasternak elastic medium using nonlocal elasticity theory and differential quadrature method, *Computational Materials Science*, 50, 2010, 239–45.
- [51] Akgöz, B., Civalek, Ö., Free vibration analysis for single-layered graphene sheets in an elastic matrix via modified couple stress theory, *Materials and Design*, 42, 2012, 164–71.
- [52] Mohammadi, M., Ghayour, M., Farajpour, A., Free transverse vibration analysis of circular and annular graphene sheets with various boundary conditions using the nonlocal continuum plate model, *Composites Part B: Engineering*, 45, 2013, 32–42.
- [53] Asemi, S.R., Farajpour, A., Decoupling the nonlocal elasticity equations for thermo-mechanical vibration of circular graphene sheets including surface effects, *Physica E*, 60, 2014, 80–90.
- [54] Ansari, R., Mohammadi, V., Shojaei, M.F., Gholami, R., Sahmani, S., Surface stress effect on the post-buckling and

- free vibrations of axisymmetric circular Mindlin nanoplates subject to various edge supports *Composite Structures*, 112, 2014, 358–67.
- [55] Pradhan, S.C., Murmu, T., Small scale effect on the buckling analysis of single-layered graphene sheet embedded in an elastic medium based on nonlocal plate theory, *Physica E*, 42, 2010, 1293–301.
- [56] Malekzadeh, P., Setoodeh, A.R., Alibeygi, A., Small scale effect on the thermal buckling of orthotropic arbitrary straight-sided quadrilateral nanoplates embedded in an elastic medium, *Composite Structures*, 93, 2011, 2083–9.
- [57] Karamooz Ravari, M.R., Shahidi, A.R., Axisymmetric buckling of the circular annular nanoplates using finite difference method, *Meccanica*, 48, 2013, 135–144.
- [58] Bedroud, M., Hosseini-Hashemi, S., Nazemnezhad, R., Buckling of circular/annular Mindlin nanoplates via nonlocal elasticity, *Acta Mechanica*, 224, 2013, 2663–76.
- [59] Farajpour, A., Mohammadi, M., Shahidi, A.R., Mahzoon, M., Axisymmetric buckling of the circular graphene sheets with the nonlocal continuum plate model, *Physica E*, 43, 2011, 1820–5.
- [60] Golmakani, M.E., Rezatalab, J., Nonuniform biaxial buckling of orthotropic nanoplates embedded in an elastic medium based on nonlocal Mindlin plate theory, *Composite Structures*, 119, 2015, 238–250.
- [61] Farajpour, A., Dehghany, M., Shahidi, A.R., Surface and nonlocal effects on the axisymmetric buckling of circular graphene sheets in thermal environment, *Composites Part B: Engineering*, 50, 2013, 333–43.
- [62] Golmakani, M.E., Vahabi, H., Nonlocal buckling analysis of functionally graded annular nanoplates in an elastic medium with various boundary conditions, *Microsystem Technologies*, 23, 2017, 3613–3628.
- [63] Golmakani, M.E., Rezatalab, J., Nonlinear bending analysis of orthotropic nanoscale plates in an elastic matrix based on nonlocal continuum mechanics, *Composite Structures*, 111, 2014, 85–97.
- [64] Golmakani, M.E., Sadraee Far, M.N., Nonlinear thermo-elastic bending behavior of graphene sheets embedded in an elastic medium based on nonlocal elasticity theory, *Computers and Mathematics with Applications*, 72, 2016, 785–805.
- [65] Sobhy, M., Thermomechanical bending and free vibration of single-layered graphene sheets embedded in an elastic medium, *Physica E*, 56, 2014, 400–9.
- [66] Sedighi, H. M., Size-dependent dynamic pull-in instability of vibrating electrically actuated microbeams based on the strain gradient elasticity theory, *Acta Astronautica*, 95, 2014, 111–123.
- [67] Sedighi, H. M., Koochi, A., Daneshmand, F., Abadyan, M., Non-linear dynamic instability of a double-sided nano-bridge considering centrifugal force and rarefied gas flow, *International Journal of Non-Linear Mechanics*, 77, 2015, 96–106.
- [68] Sedighi, H. M., Bozorgmehri, A., Dynamic instability analysis of doubly clamped cylindrical nanowires in the presence of Casimir attraction and surface effects using modified couple stress theory, *Acta Mechanica*, 227(6), 2016, 227–1575.
- [69] Ouakad, H. M., Sedighi, H. M., Younis, M. I., One-to-One and Three-to-One Internal Resonances in MEMS Shallow Arches, *Journal of Computational and Nonlinear Dynamics*, 12(5), 2017, 051025.
- [70] Koochi, A., Sedighi, H. M., Abadyan, M. R., Modeling the size-dependent pull-in instability of beam-type NEMS using strain gradient theory, *Latin American Journal of Solids and Structures*, 11, 2014, 1679–7825.
- [71] Dastjerdi, Sh., Jabbarzadeh, M., Nonlinear bending analysis of bilayer orthotropic graphene sheets resting on Winkler-Pasternak elastic foundation based on nonlocal continuum mechanics, *Composites Part B: Engineering*, 87, 2016, 161–75.
- [72] Xu, Y.-M., Shen, H.-S., Zhang, C.-L., Nonlocal plate model for nonlinear bending of bilayer graphene sheets subjected to transverse loads in thermal environments, *Composite Structures*, 98, 2013, 294–302.
- [73] Pradhan, S.C., Phadikar, J.K., Small scale effect on vibration of embedded multilayered graphene sheets based on nonlocal continuum models, *Physics Letters A*, 373, 2009, 1062–9.
- [74] Ansari, R., Rajabiehfard, R., Arash, B., Nonlocal finite element model for vibrations of embedded multi-layered graphene sheets, *Computational Materials Science*, 49, 2010, 831–8.
- [75] Jomehzadeh, E., Saidi, A.R., A study on large amplitude vibration of multilayered graphene sheets, *Computational Materials Science*, 50, 2011, 1043–51.
- [76] Pouresmaeeli, S., Fazelzadeh, S.A., Ghavanloo, E., Exact solution for nonlocal vibration of double orthotropic nanoplates embedded in elastic medium, *Composites Part B: Engineering*, 43, 2012, 3384–90.
- [77] Anjomshoa, A., Shahidi, A.R., Hassani, B., Jomehzadeh, E., Finite element buckling analysis of multilayered graphene sheets on elastic substrate based on nonlocal elasticity theory, *Applied Mathematical Modeling*, 38, 2014, 5934–55.
- [78] Murmu, T., Sieng, J., Adhikari, S., Arnold, C., Nonlocal buckling of double-nanoplate-systems under biaxial compression, *Composites Part B: Engineering*, 44, 2014, 84–94.
- [79] Radic, N., Jeremic, D., Trifkovic, S., Milutinovic, M., Buckling analysis of double-orthotropic nanoplates embedded in Pasternak elastic medium using nonlocal elasticity theory, *Composites Part B: Engineering*, 61, 2014, 162–71.
- [80] Golmakani, M.E., Sadraee Far, M.N., Buckling analysis of biaxially compressed double-layered graphene sheets with various boundary conditions based on nonlocal elasticity theory, *Microsystem Technologies*, 23(6), 2017, 2145–2165.
- [81] Asemi, S.R., Farajpour, A., Borghei, M., Hassani, A.H., Thermal effects on the stability of circular graphene sheet via nonlocal continuum mechanics, *Latin American Journal of Solids and Structures*, 11, 2014, 704–24.
- [82] Bellman, R.E., Casti, J., Differential quadrature and long-term integration, *Journal of Mathematical Analysis and Applications*, 34, 1971, 235–8.
- [83] Bellman, R.E., Kashef, B.G., Casti, J., Differential Quadrature: A Technique for the Rapid Solution of Nonlinear Partial Differential Equation, *Journal of Computational Physics*, 10, 2018, 40–52.

- [84] Mahinzare, M., Ranjbarpur, H., Ghadiri, M., Free vibration analysis of a rotary smart two directional functionally graded piezoelectric material in axial symmetry circular nanoplate, *Mechanical Systems, and Signal Processing*, 100, 2018, 188-207.
- [85] Mahinzare, M., Jannat Alipour, M., Sadatsakkak, S. A., Ghadiri, M., A nonlocal strain gradient theory for dynamic modeling of a rotary Thermo piezoelectrically actuated nano FG circular plate, *Mechanical Systems and Signal Processing*, 115, 2019, 323-337.
- [86] Watson, D. W., Karageorghis, A., Chen, C. S., The radial basis function-differential quadrature method for elliptic problems in annular domains, *Journal of Computational and Applied Mathematics*, 363, 2020, 53-76.
- [87] Lal, R., Saini, R., Vibration analysis of FGM circular plates under non-linear temperature variation using generalized differential quadrature rule, *Applied Acoustics*, 158, 2020, 107027.

ORCID iD

M.E. Golmakani  <https://orcid.org/0000-0002-0080-7168>

M. Malikan  <https://orcid.org/0000-0001-7356-2168>



© 2020 by the authors. Licensee SCU, Ahvaz, Iran. This article is an open access article distributed under the terms and conditions of the Creative Commons Attribution-NonCommercial 4.0 International (CC BY-NC 4.0 license) (<http://creativecommons.org/licenses/by-nc/4.0/>).

How to cite this article: Ahmad Pour M., Golmakani M.E., Malikan M. Thermal Buckling Analysis of Circular Bilayer Graphene Sheets Resting on an Elastic Matrix Based on Nonlocal Continuum Mechanics, *J. Appl. Comput. Mech.*, 7(1), 2021, x-xx. <https://doi.org/10.22055/JACM.2019.31299.1859>

Corrected Proof